

Desorption and diffusion at pulsed-laser-melted surfaces: The case of chlorine on silicon

Bogdan Dragnea

Laboratoire de Photophysique Moléculaire du CNRS, Bâtiment 213, Université de Paris-Sud, 91405 Orsay Cedex, France

Jacques Boulmer, Jean-Pierre Budin, and Dominique Débarre

Institut d'Electronique Fondamentale, associé au CNRS, Bâtiment 220, Université de Paris-Sud, 91405 Orsay Cedex, France

Bernard Bourguignon*

Laboratoire de Photophysique Moléculaire du CNRS, Bâtiment 213, Université de Paris-Sud, 91405 Orsay Cedex, France

(Received 22 July 1996)

The kinetics of thermal desorption from an excimer-laser-melted surface, on which diffusion into the bulk competes with desorption, is numerically evaluated and compared with a variety of experimental data for the case of Cl on Si: Auger electron spectroscopy, time-of-flight mass spectrometry, secondary-ion-mass spectrometry, and transient reflectivity. The model calculations involve nonequilibrium thermal diffusion, phase transition, segregation, and first- and second-order desorption kinetics. With the assumption that the pre-exponential factors of the desorption rates do not change on the liquid surface with respect to the solid one, activation desorption energies are found lower by ≈ 0.5 eV for the liquid surface than for the Si(100):Cl solid surface. This difference is of the order of magnitude of the latent heat of melting. The segregation coefficient of Cl at the liquid-solid interface is < 0.02 at a recrystallization speed of ≈ 6 m/s. The calculations also bring information on the dynamics of desorption and melting. The desorption rate from the liquid reaches the large value of ≈ 1 ML/ns. However, the surface is depleted from Cl atoms by both desorption and diffusion in a fraction of nanosecond (allowing only $\approx 60\%$ of the Cl to desorb). Multipulse experiments are also calculated. After only three laser pulses, only the level of Cl contamination (not the shape of the Cl depth profile) varies with laser count. The laser cleaning rate follows the laser-pulse count with a logarithmic law. It takes about five laser pulses to decrease the Cl contamination by one order of magnitude. [S0163-1829(97)06420-5]

I. INTRODUCTION

The surface melting of a solid can be easily induced by a pulsed laser at fluences lower than the ablation threshold of the material. Laser melting has been shown to be a powerful tool to induce a variety of surface modifications. These include the doping of a thin layer of a semiconductor from a gas of molecules that contain dopant atoms, the redistribution of impurities over the melted depth, the recrystallization of an amorphous layer, the etching of the substrate when it is exposed to halogen molecules, the improvement of tribological properties of metal alloys, the wetting of polymers, etc. In general, laser melting induces a strong modification of the substrate through two effects: the dramatic increase of the diffusion coefficient of impurities in the liquid phase with respect to the solid phase, and the out-of-equilibrium segregation at the rapidly moving liquid-solid interface at the recrystallization stage. These effects were studied in great details both experimentally and theoretically in the case of silicon. Because of the complexity of the process and of the evolution of the substrate during the laser pulse, a quantitative description of the experiments can only be achieved through their numerical simulation.¹⁻³ To our knowledge, desorption was not included in such calculations.

In the case of laser etching and cleaning, not only diffusion and segregation play an important role, but also does the desorption of impurities. For example, the rate of desorption of silicon chlorides may reach 0.4 ML per laser pulse on Si (Ref. 4) [here we define $1 \text{ ML} = 6.78 \times 10^{14} \text{ cm}^{-2}$, the den-

sity of Si atoms in a (100) plane]. Some dopants like Sb can also desorb from Si, but their desorption yield over a single laser pulse is much smaller than 1 ML.⁵ We have experimentally studied the laser etching of silicon by chlorine, showing that desorption and diffusion compete in that case;⁶ as a result, all Cl atoms are not "used" for etching; an important fraction of them is pumped away from the surface to the volume; these Cl atoms are nevertheless found at, or very close to, the surface after recrystallization, due to a strong segregation of Cl at the liquid-solid interface. In this paper we report the numerical simulation of the experiments of Ref. 6. In addition to laser heating, surface melting, diffusion, and segregation of the impurities, the simulation includes the desorption of silicon chlorides. The segregation coefficient of Cl, the desorption kinetics of silicon chlorides, and the evolution of the substrate during the laser pulse, are deduced from the comparison of the calculations with the experimental data.

A finite-difference approximation is used to solve numerically the heat and mass flow equations.⁷ The desorption rates are written according to the Polanyi-Wigner rate equation

$$\dot{\Theta} = \nu \Theta^n \exp(-E^a/kT), \quad (1)$$

where k is the Boltzmann constant, Θ is the adsorbate coverage, T is the surface temperature, E^a is the activation energy of desorption, ν is the pre-exponential factor and n is the reaction order. Both first and second orders in Cl coverage are considered. Depending on the solid or liquid state of

TABLE I. Experimental data and calculated results for the case of “coupled” kinetics (see text, Sec. III C). Θ_{AES} and n_{SIMS} are the “surface Cl” and Cl concentrations in the eighth plane below the surface after the laser pulse, respectively. SiCl/SiCl₂ is the branching ratio between the desorption products. K_s is the segregation coefficient.

	E_1^s (eV)	E_1^l (eV)	E_2^l (eV)	E_2^s (eV)	Θ_{AES} (ML)	SiCl/SiCl ₂	Etch rate (Å/pulse) ^a	n_{SIMS} (10 ¹⁹ cm ⁻³)	K_s
This work	2.7 ^b	2.0±0.1 ^b	3.3±0.1 ^c	3.7±0.1 ^b	0.39	0.95	0.55	0.8	≤0.02
Experiment	2.45			3.61	0.37±0.13	1.3±0.3 Ref. 7	0.56±0.04	≤1.0	
	Ref. 9			Ref. 8	Ref. 6		Ref. 6	Ref. 6	

^aFor laser fluences above 500 mJ cm⁻².

^bAssuming a preexponential factor of 10¹⁴ s⁻¹.

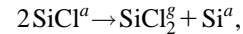
^cAssuming a preexponential factor of 2×10³ cm² s⁻¹.

the surface, and on the reaction order (1 or 2), E^a is written $E_{1/2}^{s/l}$. In order to compare the results of calculations with a variety of experimental data, the computer program allows for multiple pulse irradiation, for readsorption of Cl between or during laser pulses, and for the etching of the surface. At the end of a pulse, the final density profile, possibly modified by readsorption, becomes the initial density distribution for the next pulse. Inputs to the program include the number of pulses, the initial Cl depth profile, the time evolution of the surface temperature, and of the melted depth as tables. Fitted parameters are the segregation coefficient and the activation energies of first- and second-order desorption. The diffusion coefficient of Cl in liquid Si is taken to be 1.6×10^{-4} cm² s⁻¹, which is an average of the diffusion coefficient reported for other impurities or dopants of Si;⁵ diffusion does not depend very much on the nature of the impurity. Pre-exponential factors were taken to be 2×10^3 cm² s⁻¹ and 10^{14} s⁻¹ for second- and first-order desorption, respectively.^{8,9} These values are “normal” for desorption, and we did not attempt to determine them.

The simulations are compared with time-of-flight (TOF) mass spectrometry results on the desorption products, with Auger-electron-spectroscopy (AES) data of the undesorbed Cl atoms and secondary-ion-mass-spectrometry (SIMS) data of the Cl distribution in the bulk. The results of Ref. 6 which are used for comparison with our calculations are summarized in Table I. Under experimental conditions where no gas phase molecules interact with the surface during the laser pulse, the etch rate saturates at ≈ 0.56 Å/pulse, or ≈ 0.40 ML of Si.⁴ In Ref. 6, the Si is divided arbitrarily in two regions: region I consists of the seven atomic planes nearest to the surface, and region II is below region I. In what follows, Cl in region I (expressed in ML) is called “surface Cl”, while “bulk Cl” stands for Cl in region II. By AES it was found that the surface chlorine is $\Theta_{\text{AES}} = 0.37 \pm 0.10$ ML after one laser pulse, and the SIMS depth profile shows less than 10¹⁹-cm⁻³ bulk chlorine. The branching ratio between the main desorption products (SiCl/SiCl₂) was found close to unity in TOF measurements. These results are for a laser fluence of 600 mJ cm⁻², and we refer to this value in the following unless otherwise mentioned. In addition, the calculations are compared with the relative desorption yield of SiCl in a series of laser pulses following one single chlorine dose (TOF measurements) and with the Cl depletion in region I as probed by AES as a function of laser count.

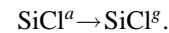
Several experimental studies give a rather extensive description of Cl adsorption on solid Si(100) surfaces, as well

as of the thermal-desorption kinetics of chlorosilicon molecules. Cl₂ adsorbs dissociatively on Si(100) onto the top silicon layer and a high-energy barrier hinders the bulk penetration.¹⁰ X-ray-photoemission-spectroscopy studies show that the surface species is mainly SiCl,¹¹⁻¹⁴ and a saturation coverage of ≈ 1 ML was found. The desorption product is mainly SiCl₂ for the solid surfaces. Various orders of the desorption kinetics were found depending on the Cl coverage:⁸ the surface structure, the surface diffusion, and the lateral interactions account for the observed variations. The desorption reaction of SiCl₂ from a monochlorinated surface implies the formation of dichloride from two SiCl: the reaction order may be 2, when SiCl are randomly distributed on the surface and diffuse to give SiCl₂; or 1 under some circumstances, for instance when preparing of Cl atoms on the surfaces occurs. The latter was observed on solid surfaces by molecular-beam studies⁸ for chlorine coverages smaller than 0.4 ML. The desorption may be written as



where the upper index indicate the adsorbed phase or the gas phase. For etched surfaces the reaction rate showed a second-order dependence on chlorine coverage for all coverages.⁸ The activation energy of second-order desorption in this case is reported⁸ to be $E_2^s = 3.61$ eV for a pre-exponential factor of 2×10^3 cm² s⁻¹ (Table I).

SiCl is also reported to desorb from the solid, but at higher temperatures (above 900 °C).^{8,9,15} The desorption may be described by a first-order equation



The activation energy of first-order desorption was reported to be $E_1^s = 2.45$ eV using a Readhead analysis,⁹ and a pre-exponential factor of 10¹³ s⁻¹.

As stated above, the product yields of the excimer laser-induced desorption following a pulsed adsorption of Cl₂ were reported in Ref. 6. SiCl is at least as abundant as SiCl₂, unlike the case of the thermal-programmed-desorption and LITD (laser induced thermal desorption) conditions, where SiCl₂ is the major desorption product.^{8,16} Thus, the experimental conditions (heated solid surface or laser melted surface) significantly change the surface chemistry as will be discussed in this paper.

The paper is organized in six sections. In Sec. II, we describe the thermal model of laser melting used to calculate the melting dynamics. The description of the model of mass

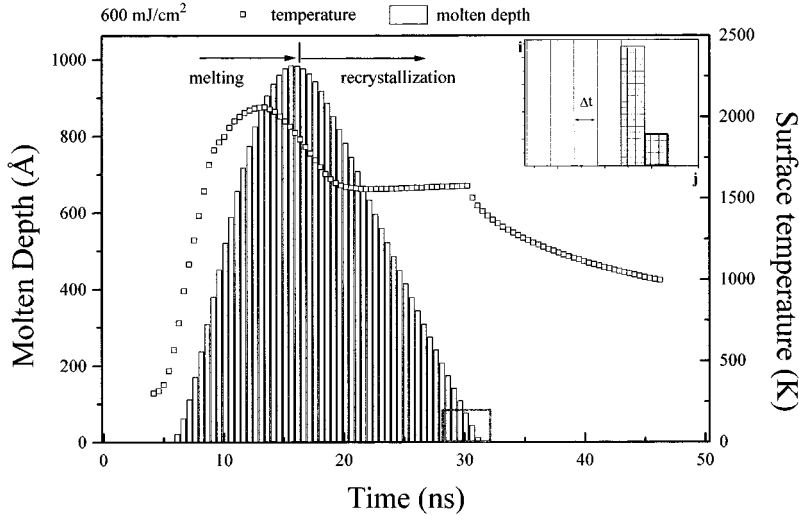


FIG. 1. Calculated surface temperature (squares) and melted depth (bars) for a laser pulse of fluence 600 mJ cm^{-2} and of a FWHM of 11 ns at 308 nm on a silicon substrate. In the inset are sketched the space and time divisions in the quasi-stationary finite-difference approximation: i and j stand for the space and time step numbers, respectively. The calculated molten depth and surface temperature are sampled in Δt -wide time cells.

transport and segregation is given in Sec. III together with a comparison with previous similar calculations and experiments of nonequilibrium dopant incorporation.^{3,5} In Sec. IV, we present the results of our calculations: the etch rate, the remaining chlorine depth profile, the evolution of the chlorine concentration at the surface during the laser pulse, and the effect of multiple pulse irradiation. Section V contains a discussion of the results. Finally, we conclude with a brief summary of the results and the possible extensions of this work in Sec. VI.

II. CALCULATION OF HEAT DIFFUSION AND MELTING DYNAMICS

In this work, heat diffusion and impurity diffusion are calculated separately. The output of the heat diffusion calculation (temperature and melted depth vs time) is used as an input of the impurity diffusion program.

Laser heating of the substrate is calculated using the classical heat diffusion equation. It is assumed that electron transport is negligible as compared to heat transport, and that the conversion of the laser-induced electronic excitation into heat is very fast at the time scale of the laser pulse. We use the equation

$$\frac{\partial}{\partial t} (\rho c T(z, t)) = \frac{\partial}{\partial z} \left(K \frac{\partial T(z, t)}{\partial z} \right) + S(z, t) + M(z, t), \quad (2)$$

where T is the temperature, z is the depth, and ρ , c , and K are the Si density (g cm^{-3}), heat capacity (J g^{-1}), and thermal conductivity ($\text{J s}^{-1} \text{cm}^{-1} \text{K}^{-1}$). These three parameters are related to the diffusion coefficient D ($\text{cm}^2 \text{s}^{-1}$) by the relationship $D = K/\rho c$. S and M are the terms corresponding to the source of energy (i.e., laser absorption) and to the latent heat of melting, respectively. The one-dimensional form of the heat equation is used because the lateral dimension of the laser beam ($\approx 2 \text{ mm}$) is much larger than the heat diffusion length at the time scale of the laser pulse ($\approx 1 \mu\text{m}$).

The equation has been used by various authors.^{1,3,17} In general, the left-hand term is written in the form $\rho c (\partial/\partial t) T(z, t)$. But we do find that the term

$[\partial(\rho c)/\partial t] T(z, t)$ has to be included in the calculation in order to achieve energy conservation when temperature-dependent parameters are used (which is necessary to describe the heating of a semiconductor). Typically, an excess of heat equal to $\approx 4\%$ of the absorbed laser energy is found in the material after 50 ns when the term is not included, for a laser fluence of 500 mJ cm^{-2} (which is above the melting threshold).

The equation has been solved numerically by an explicit method. In order to keep the calculating time within reasonable limits, the Si is divided in slices, the size of which increase geometrically by a factor of 1.1 at each slice. The surface slab is 40 \AA thick. A smaller thickness was found to change the maximum surface temperature of only a few degrees K, for laser fluences resulting in temperatures above the equilibrium melting temperature of 1683 K. The thermal parameters of Si are taken from Ref. 17. Overheating of the solid phase, and undercooling of the melted phase, are included in our code.¹⁸ The variation of the effective melting temperature T_f with the speed of the melting and recrystallization front, v is phenomenologically described by the relationship $\Delta T_f = \zeta v$, where ζ has the value $17 \text{ K m}^{-1} \text{ s}$ for Si.¹⁸ Typically, including overheating and undercooling results in an increase of the calculated melting duration of $\approx 10\%$. The melted depth is also larger by a similar amount. The calculated melting (recrystallization) temperature is larger (smaller) than the equilibrium value by $\approx 100 \text{ K}$. The surface temperature and the melted depth are shown in Fig. 1 for a laser fluence of 600 mJ cm^{-2} .

Our computer code was tested under conditions where the result can be compared with an analytical solution, namely, when the surface is put in contact at $t=0$ with a heat source that is held at a fixed temperature (and using temperature-independent parameters). The energy balance is checked at the end of every calculation by integrating the heat present in the material, which is compared to the energy that was absorbed during the laser pulse.

Our code allows a satisfactory comparison with the experimental results of Ref. 17. However, while this sort of calculation is a good tool to study the dependence of laser melting on a given experimental parameter like the laser fluence, we do not consider that it has the capability of absolute

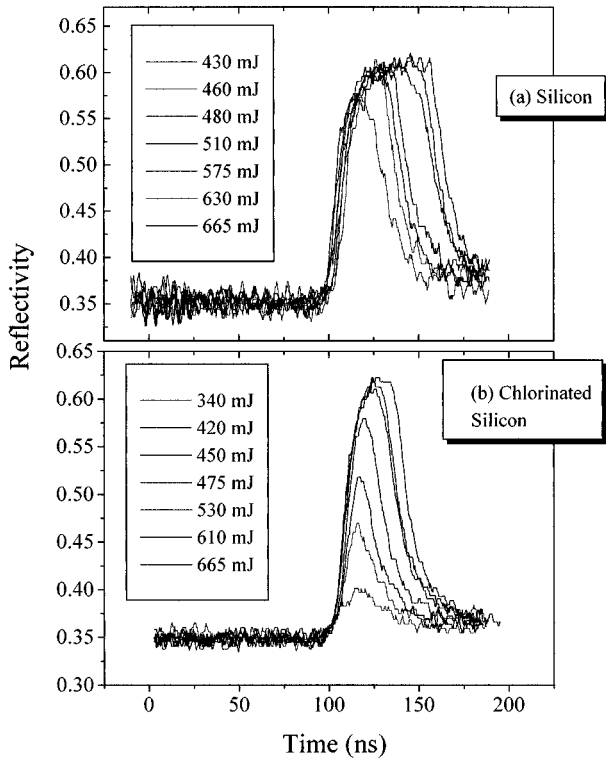


FIG. 2. Experimental transient reflectivity records at 633 nm, induced on silicon by the exposure to an excimer laser beam at 308 nm: (a) for a “clean” Si surface [held in a secondary vacuum environment (10^{-7} mbar)], and (b) for a saturated Si:Cl surface (same base pressure, pulsed Cl_2 molecular beam and ambient pressure of 10^{-6} mbar of chlorine). The laser fluences are indicated on the left of the figures. The height and width of the transients increase with laser fluence. The onset of the transient occurs earlier as the fluence increases.

predictions. This is mainly because the thermal and optical parameters of silicon above 1000 K were determined from the comparison of the present type of calculation with laser heating and/or melting experiments, where the melting duration and depth are measured; the problem is that the experimental melting duration and depth of Si, which are used to fit the optical and thermal properties, depend significantly on the ambient gas of Si, which is not controlled in most reported experiments. The parameters up to 1000 K were determined in air by ellipsometry.¹⁹ This point is illustrated in Fig. 2. Reflectivity transients of Si at 638 nm are displayed for Si in a secondary vacuum (10^{-7} mbar), and in a chlorine environment (same base pressure, pulsed molecular beam of chlorine directed toward the surface, and ambient chlorine gas at 10^{-6} mbar). The difference between the two experiments is much larger than the experimental uncertainty; by contrast, the transients of Fig. 2 obtained for a chlorine environment are very similar to those obtained in a previous work from our laboratory, in which the experimental setup was entirely different.²⁰ This shows that the results are quite reproducible, and that the melting dynamics depend strongly on the adsorbed molecules.

We do not attempt to solve this problem in this work. This would imply modeling the change of thermal and optical properties of Si induced by impurities, and incorporating this

model into the code describing laser heating and melting. In addition, heat and impurity diffusion would have to be calculated together. This is beyond the scope of this paper, which is to unravel the basic features of the desorption dynamics during laser melting. Our method is to calculate laser heating and melting for a range of laser fluences, using the “clean Si” parameters of Ref. 17; for a given *experimental* laser fluence, in the mass transport program we use the temperature transient that is obtained for the fluence that yields the right melted depth. In other words, we use the laser fluence as a scaling parameter. The experimental melted depths are obtained by measuring B depth profiles as measured after laser etching experiments by SIMS.⁵ We choose B because we do not observe a change of the melting duration and depth with the density of B in Si.

III. MASS TRANSPORT, DIFFUSION, SEGREGATION, AND DESORPTION

A. Definition of the model. Initial value problem.

Finite-difference equations

Because the diffusion coefficient in solids is seven orders of magnitude less than in the liquid phase, we neglect the diffusion from the surface into the solid. During melting, the system is described as a one-dimensional liquid with two moving borders: the free liquid-vacuum (LV) border moves at the etching velocity toward deeper locations, and the liquid-solid (LS) border propagates first inwards during melting, then outwards during recrystallization. We choose the one-dimensional treatment because the heat diffusion length is much smaller ($\sim 1 \mu\text{m}$) than the size of the laser ($\sim 2 \text{mm}$). Chlorine is the solute in this moving fluid. Convection is not included in the model. The etching velocity is taken into account only for a repeatedly irradiated surface with a large number of pulses since the etch rate does not exceed 0.56 \AA/pulse ,⁶ which is much smaller than the spatial resolution of $\approx 9 \text{ \AA}$ that we use in our calculations.

Space and time are divided in cells indexed by i and j , respectively (Fig. 1). The length of time cells is Δt . At the time $t = j\Delta t + \Delta t/2$ corresponds a melted depth $z_{\text{LS}}(j)$ and a surface temperature provided by the thermal diffusion calculations described in Sec. II. For a time interval Δt sufficiently small, the molten depth is considered constant. The diffusion equation with the Cl depth profile for $j-1$ as initial value is solved in the cell j over the depth $z_{\text{LS}}(j)$ (Fig. 1). Melting or solidification occurs, resulting in a change of z_{LS} , and a new diffusion problem is solved in the cell $j+1$, with the initial conditions given by the final state of the former cell j .

The diffusion equation is

$$\frac{\partial n}{\partial t} = \frac{\partial}{\partial z} \left(D \frac{\partial n}{\partial z} \right), \quad (3)$$

with $n(z, t)$ the Cl density in the liquid phase at time t and depth z , and D the diffusion coefficient. In the finite-difference approximation, the equation has the form $n_{j+1}^i - n_j^i = r(n_{j-1}^{i-1} - 2n_j^i + n_j^{i+1})$, where $r = D(\Delta t/\Delta z^2)$.

At the LV border, the desorption of silicon chlorides occurs at the same time as the diffusion into the bulk. The continuity equation reads

$$\frac{dn}{dt} = \frac{\partial n}{\partial t} + \nabla \cdot \mathbf{J} = f(n), \quad (4)$$

where \mathbf{J} is the flux across the surface, and $f(n)$ is the desorption rate. Since no mass transport occurs through the surface, but desorption, we have $\nabla \cdot \mathbf{J} = 0$. When coupled with the diffusion equation (3), the free border condition becomes, in the finite-difference approximation

$$n_j^0 - n_j^{-1} = 0, \quad (5)$$

$$n_{j+1}^0 - n_j^0 = f(n)dt + r(n_j^{-1} - 2n_j^0 + n_j^1),$$

$i=0$ corresponds to the surface layer, and $i=-1$ is a layer in vacuum. The surface coverage Θ is related to the volume density n by the equation

$$\Theta = n_{\text{Cl}}/n_{\text{Si}(z=0)}. \quad (6)$$

B. Segregation during recrystallization

There are different equations at the LS border for melting and recrystallization. At the melting stage the flow across the LS interface is zero, since the diffusion coefficient in the solid is negligible: $\partial n/\partial z = 0|_{z=z_i}$, with z_i , the interface position or, in the finite-difference form, $n_j^i - n_j^{i-1} = 0$.

When Si solidifies, Cl is rejected from the solid to the liquid phase. Segregation occurs at conditions far from equilibrium, and is characterized by a coefficient K_s which in general is a function of the interface velocity v_r .²¹ K_s is defined by the conservation law at the recrystallization front:³

$$\frac{\partial n}{\partial z} + (1 - K_s)v_r \cdot n = 0. \quad (7)$$

The flux of impurity atoms that cross the interface is $v_r(n_L - n_S)$. One can readily observe that $1 - K_s$ must behave as $1/v_r$ in order to account for the fact that segregation is most efficient for $v_r \rightarrow 0$. Therefore, when Eq. (7) is used as a Neumann (or derivative) boundary condition one has to model the velocity dependence of solute partitioning. However, in some cases, the segregation is so strong that the resulting impurity concentration is not measurable by the usual experimental methods (SIMS and Rutherford backscattering). Using such a model is then not sensible, because it cannot be compared with experiment. This is precisely the case of chlorine on silicon. Therefore, we use in this work a segregation coefficient K_s given by $K_s = n_S/n_L$, maintained constant all along the calculations.²

The mass transport associated with segregation takes place in a layer of thickness $v_r \Delta t$. We impose that the final average concentration in this interface layer is uniformly taken as K_s times the initial average concentration of the solute (Cl) in the liquid solvent (Si). The concentration in excess is transferred to the nearest liquid layer. This implies the assumption that the segregation takes place much faster than diffusion. This is reasonable for systems such as Cl/Si for which segregation is found strong,⁶ but it is not true in general. According to this picture, when $v_r \Delta t \rightarrow 0$, a single layer recrystallizes during Δt , and the average condition becomes the local condition: $n_S/n_L = K_s$.

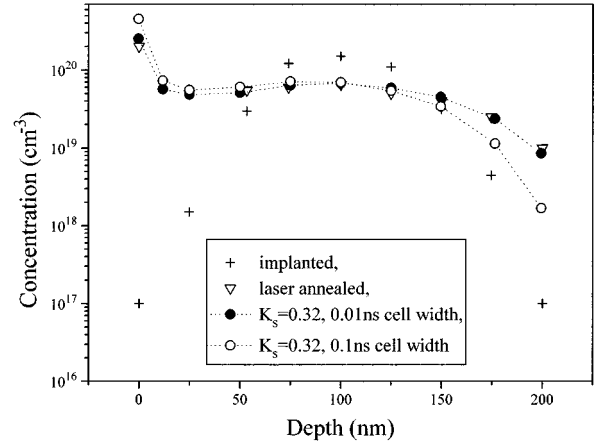
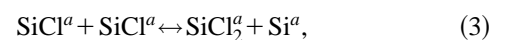
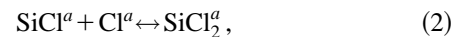


FIG. 3. Depth profiles of Bi in Si, as implanted and after laser annealing. Experimental data after Ref. 2. The results of two calculations are shown, corresponding to time resolutions of 0.1 and 0.01 ns.

We have tested our approach to segregation on a number of depth profiles of dopant distribution in laser-annealed Si, as found in Campisano and Wood's works. The result of our calculation for Bi in Si is shown in Fig. 3. There is no Bi desorption, so the calculation includes only the dopant redistribution. As already stated, the definition of the interfacial distribution coefficient is applied on average to the set of layers which is crossed by the recrystallization front during one temporal step. Thus the solute quantity rejected into the liquid is proportional to the thickness of this set of layers, and in turn to the time duration of the chosen temporal step. Therefore the results will depend somewhat on the adopted time resolution. It is worth noting that the required time step for a good accuracy is generally smaller than the one required by the stability condition in the explicit method; therefore there is no significant improvement of the calculation time with the implicit method used here with respect to the explicit method. Nevertheless, we choose this approximation because it does not bring numerical instabilities, and it allows us to reach accurate enough results in a reasonable computing time. We find that the results obtained for different temporal resolutions do converge more or less rapidly depending on the segregation coefficient. As expected, the approximation is better for smaller K_s .

C. Desorption from the liquid surface

The possible chemical states of chlorine on a molten Si surface are not known precisely. Si atoms, Cl atoms, and SiCl_x molecules ($x=1$ and 2) may coexist, and the following chemical equilibria may be considered:



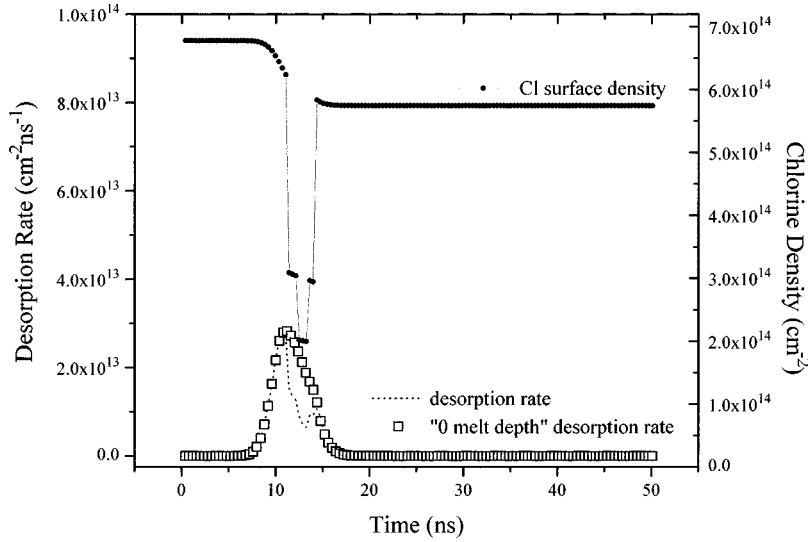


FIG. 4. Calculated desorption rate and surface Cl density as functions of time during surface melting. The parameters used in the calculation are first-order desorption, 350 mJ cm^{-2} , $K_s = 0.02$, and $E_1^l = E_1^s = 2.15 \text{ eV}$. The desorption rate, as calculated by freezing the diffusion to the bulk, is also shown for comparison ("0 melt depth") on the figure.



We do not consider SiCl_x with $x=3$ and 4 (although their formation is exothermal) because these molecules are not observed to desorb. At the beginning of melting, most Cl atoms are in the form SiCl^a . Since SiCl is a strongly bound molecule ($\approx 5 \text{ eV}$ in the gas phase) the dissociation following Eq. [1] should not be important even at the peak temperature of $\approx 2000 \text{ K}$. As a result Eq. [3] rather than Eq. [2] must be considered for the formation of SiCl_2 . As for Eq. [1], the formation of SiCl_2 should be dominant in Eq. [2] (Eqs. [1] and [2] are strongly exothermic from left to right).

Reaction [3] may be exothermal or endothermal. From left to right, it may be limited by diffusion, while it will not be from right to left. At the very beginning of melting, when Cl atoms are all at the surface, diffusion should not limit the rate and reaction [3] should occur easily from left to right. Later, as the chlorinated species are desorbed or dispersed by diffusion over an increasing volume, diffusion should limit strongly the production of SiCl_2 , while the dissociation of SiCl_2 by the reverse reaction will occur at a constant rate. Reactions [4] and [5] do not occur at a comparable rate on the solid surface, where most desorption occurs through reaction [5], although the main surface species is SiCl . We assume that this does not change on the liquid surface: Eq. [5] would be fast, while Eq. [4] would be slow.

(1) "Coupled" kinetics. Let us assume that the SiCl_2 concentration and coverage remain significantly smaller than the SiCl ones (because reaction [5] is faster than reaction [3], and because the reverse of reaction [3] is not negligible, so that SiCl_2 molecules which have diffused to, or were formed in, the bulk dissociate in the bulk rather than reach the surface and desorb). With these assumptions, we obtain

$$\frac{d[\text{SiCl}^g]}{dt} = k_4[\text{SiCl}^a], \quad (8)$$

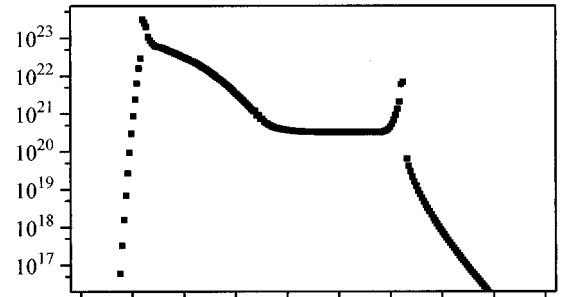
$$\frac{d[\text{SiCl}_2^g]}{dt} = k_5[\text{SiCl}_2^a] = k_3[\text{SiCl}^a]^2. \quad (9)$$

SiCl and SiCl_2 kinetics are coupled, the SiCl desorption is first order in Cl coverage, and the SiCl_2 desorption is second order in Cl coverage, the Cl coverage Θ being

$$\Theta = [\text{Cl}^a] + [\text{SiCl}^a] + 2[\text{SiCl}_2^a] \approx [\text{SiCl}^a]. \quad (10)$$

In this case, the branching ratio BR (integrated over the melting duration) is

Desorption Rate (atoms $\text{cm}^{-2} \text{ s}^{-1}$)



Chlorine surface density (cm^{-2})

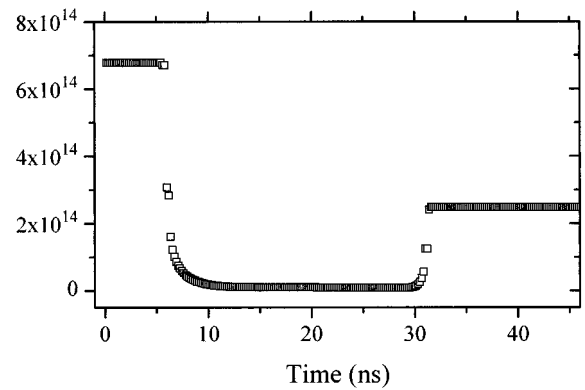


FIG. 5. Calculated desorption rate and chlorine coverage as a function of time during laser melting; the parameters used in the calculation are second-order desorption, 600 mJ cm^{-2} , $K_s = 0.02$, $E_2^l = 3.0 \text{ eV}$, and $E_2^s = 3.7 \text{ eV}$.

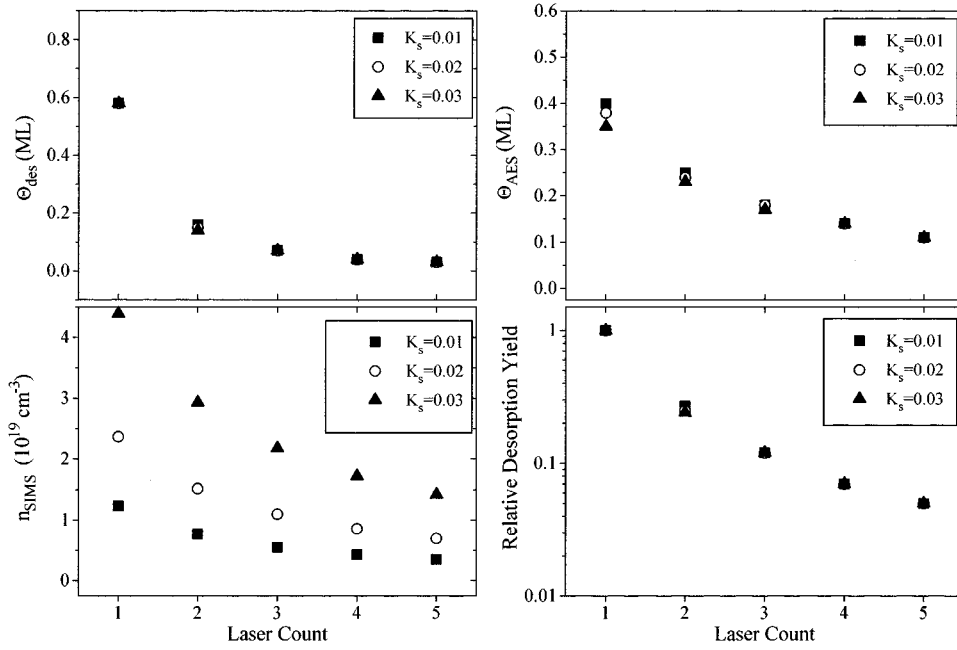


FIG. 6. Influence of the segregation coefficient K_s on (a) the Cl desorption yield (Θ_{des}), (b) the surface Cl at the end of the laser pulse (Θ_{AES}), (c) the Cl concentration in the eighth plane below the surface (n_{SIMS}), and (d) the relative desorption yield as a function of laser count. The parameters used in the calculation are second-order desorption, 600 mJ cm^{-2} , $E_2^l = 3.1 \text{ eV}$, and $E_2^s = 3.7 \text{ eV}$.

$$\text{BR} = \frac{\int k_4[\text{SiCl}^a] dt}{\int k_3[\text{SiCl}^a]^2 dt}, \quad (11)$$

where k_3 and k_4 depend on time through the temperature, and $[\text{SiCl}^a](t)$ is a function of time that involves diffusion and desorption. This branching ratio is an output of our computer program.

(2) *Separate kinetics.* If we now assume that the reverse of reaction [3] is negligible, then all the SiCl_2 molecules formed at the beginning of melting will either desorb quickly or diffuse to the bulk and ultimately desorb or stay at the surface after recrystallization when they diffuse back to the surface. The kinetics is different in this case. The branching ratio between SiCl and SiCl_2 is “decided” at the early stage of melting, while the SiCl concentration near the surface is large enough to yield a significant amount of SiCl_2 through reaction [3]. Let us note η the fraction of surface chlorine in the form of SiCl . The total coverage of chlorine is

$$\Theta = [\text{Cl}^a] + [\text{SiCl}^a] + 2[\text{SiCl}_2^a] \approx [\text{SiCl}^a] + 2[\text{SiCl}_2^a]. \quad (12)$$

The “initial” SiCl and SiCl_2 coverages are

$$[\text{SiCl}^a]_0 = \eta\Theta_0, \quad (13)$$

$$[\text{SiCl}_2^a]_0 = \frac{1}{2}(1 - \eta)\Theta_0. \quad (14)$$

The rates of desorption are

$$\frac{d[\text{SiCl}^g]}{dt} = k_4[\text{SiCl}^a], \quad (15)$$

$$\frac{d[\text{SiCl}_2^g]}{dt} = k_5[\text{SiCl}_2^a]. \quad (16)$$

The branching ratio BR is again a complicated fraction of integrals that are calculated by our program:

$$\text{BR} = \frac{\int k_4[\text{SiCl}^a] dt}{\int k_5[\text{SiCl}_2^a] dt}. \quad (17)$$

We have fitted the experimental data with first-order kinetics alone, second-order kinetics alone, and the two combinations of first- and second-order kinetics corresponding to “coupled” or “separate” kinetics.

IV. RESULTS

A. Influence of the diffusion on desorption and Cl coverage

Melting allows the adsorbate to penetrate beneath the surface, and therefore decreases the available amount of chlorine for desorption. As a result, if we use the same kinetic parameters for desorption from the solid and liquid surfaces, we expect surface melting to cause a decrease of the desorption rate, in contradiction with the experimental results. This shows that the desorption kinetics cannot be the same on the solid and the liquid, and that $E^l < E^s$.

We first do not take this fact into account, and we use the same kinetics for both states of the surface in order to show the influence of diffusion on desorption. In Fig. 4 we show the calculated desorption rate and surface coverage during a laser pulse, using a segregation coefficient of 0.02 and a first-order desorption with an activation energy of 2.15 eV. The chosen laser fluence is 350 mJ cm^{-2} , which is just above the melting threshold, the diffusion lasts a short time, and acts only as a perturbation onto desorption, and the latter remains the main process involved in the adsorbate depletion at the surface. Also shown in the figure is the result of a calculation where the value of the diffusion coefficient is kept at its value for the solid (as if the surface did not melt:

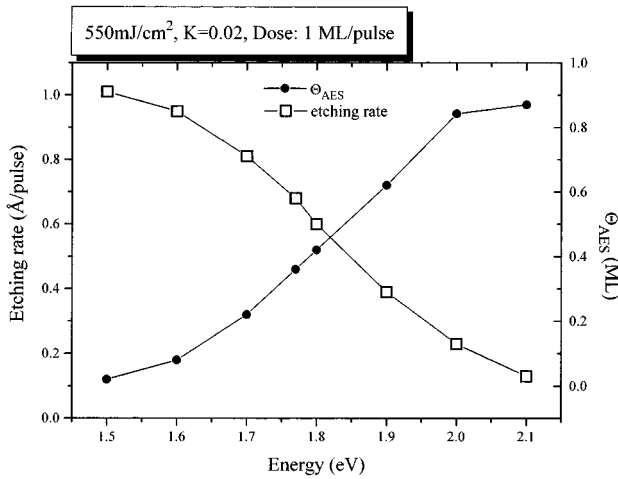


FIG. 7. Effect of the activation energy of desorption on the calculated surface chlorine after the laser pulse (Θ_{AES}), and on the etching rate. The parameters used in the calculation are first-order desorption, 550 mJ cm^{-2} , $K_s=0.02$, and $E_1^s=E_1^l$.

“0 melt depth” on Fig. 4). The comparison between the two cases shows the strong effect of Cl depletion by diffusion during surface melting. The Cl coverage decreases by a factor of ≈ 4 during melting. As a result, when melting starts, the desorption rate on the liquid surface also decreases strongly as the adsorbate penetrates into the melted silicon. Subsequently, the recrystallization pushes the diffused chlorine back to the surface, and the desorption increases again: two desorption peaks occur as a function of time.

For fluences well above the melting threshold, the surface is depleted in a fraction of nanosecond (Fig. 5), so that the desorption rate is significant only at the beginning of melting. The second peak is observable as at smaller fluence, but it is delayed, and its height is smaller than that of the first peak by nearly two orders of magnitude.

B. Influence of the segregation coefficient on desorption and Cl depth profile

One expects that the segregation does not have an important influence on desorption, since the latter occurs mainly at

the very beginning of melting (as shown in Sec. IV A) while the former takes place during the recrystallization. Indeed, the role of the segregation coefficient on the desorption yield is proportional to the height of the second desorption peak. This peak decreases as the fluence increases because the remaining Cl quantity below the surface decreases. Figure 6 shows the calculated influence of K_s on the Cl desorption yield, the remaining surface Cl, the remaining bulk Cl, and the relative desorption yield for a series of laser pulses. As expected, K_s greatly influences the bulk chlorine, but by contrast it has almost no effect on the desorption yield. The surface Cl varies only slightly with K_s ($\approx 10\%$) when the latter varies by -90 – $+100\%$. As a result, the value of K_s can be inferred from the SIMS measurements alone. The experimental upper limit of 10^{19} cm^{-3} for the Cl concentration in the bulk sets an upper limit of 0.02 for K_s .

C. Desorption kinetics

Once a satisfactory value is obtained for K_s , we use the other experimental results (namely, AES at 600 mJ cm^{-2} and the etching rate as a function of laser fluence), to derive the values of the activation energies of desorption. At low fluence, the desorption occurs on a solid surface, while for the higher fluences both states of the surface contribute to the desorption. Therefore, the two fit parameters E^s and E^l can be determined independently. An example of the choice of the appropriate fit parameters is depicted in Fig. 7 for a first-order desorption on the liquid surface and for a SiCl to SiCl₂ ratio of 1. One observes that the “etching rate” and “AES” criteria can be met together.

On the solid surface, a pure second-order kinetics yields an activation energy which agrees well with the value of the literature (Table I). A pure first-order kinetics does not agree so well (Table I). Since SiCl is a minor desorption product on the solid, in what follows we shall calculate the desorption from the solid with a second-order kinetics in chlorine coverage.

On the liquid surface, a first-order kinetics fails to reproduce the etch rate dependence on laser fluence. A plateau cannot be obtained [Fig. 8(a)] because the desorption (which

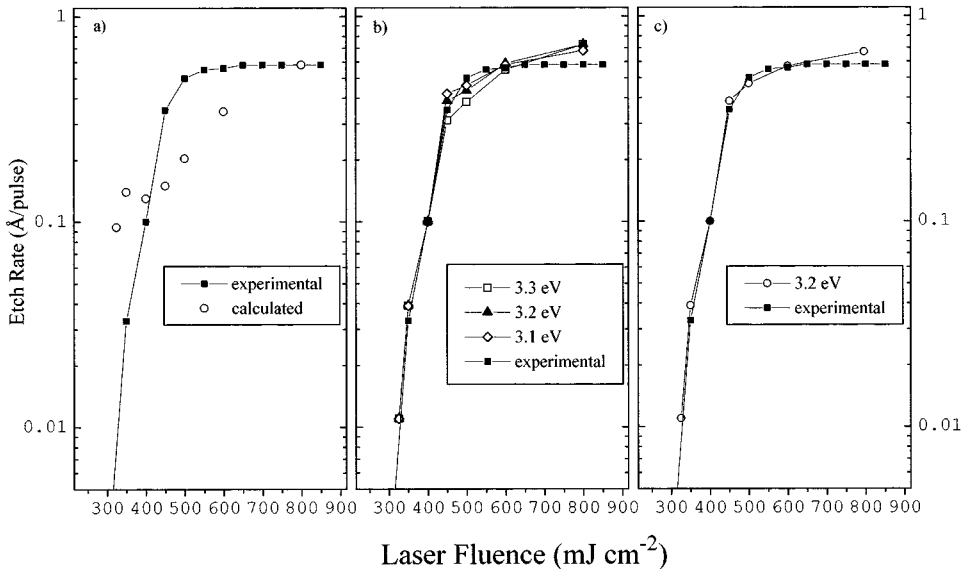


FIG. 8. Experimental and calculated etch rate dependence on laser fluence. The parameters used in the calculation are (a) first-order desorption, $K_s=0.02$, and $E_1^s=E_1^l=2.15 \text{ eV}$; (b) coupled kinetics, $K_s=0.01$, $E_2^s=3.7 \text{ eV}$, $E_1^l=2.0 \text{ eV}$, and E_2^l as indicated on the figure; and (c) separate kinetics, $K_s=0.02$, $E_2^s=3.7 \text{ eV}$, $E_1^l=2.0 \text{ eV}$, and $E_2^l=3.2 \text{ eV}$.

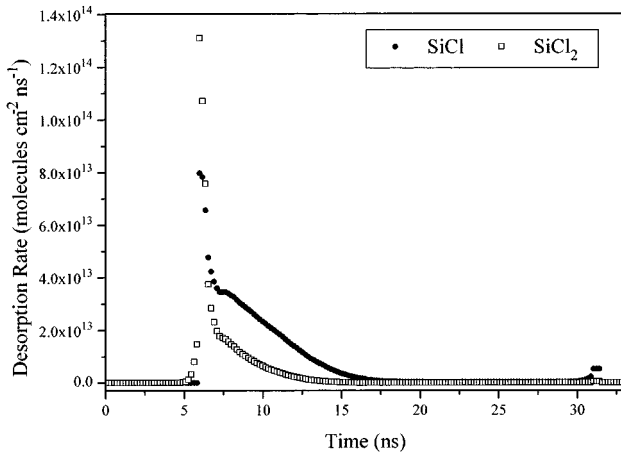


FIG. 9. SiCl and SiCl₂ desorption rates in the “coupled” desorption scheme. The parameters used in the calculation are 600 mJ cm^{-2} , $K_s = 0.01$, $E_2^s = 3.7 \text{ eV}$, $E_1^l = 1.9 \text{ eV}$, and $E_2^l = 3.3 \text{ eV}$.

increases the etch rate) is more dependent on the laser fluence than the diffusion (which decreases the etch rate): this is due to the fact that Cl atoms diffuse more slowly than heat; the increased rate of the heat diffusion induced by the increase of the laser fluence has little effect on Cl diffusion. Since a second-order kinetics cannot account for the SiCl desorption (which is first order in Cl coverage), this implies the use of a more complex kinetic frame where both second- and first-order kinetics are involved. As stated in Sec. III, we consider two kinetic models, where SiCl and SiCl₂ desorption are either “coupled” or “separate.” In the first case, the ratio of the SiCl and SiCl₂ desorption rates depends on the Cl coverage, whereas it does not in the second case.

Coupled kinetics. The desorption rates of SiCl and SiCl₂ are represented in Fig. 9 as a function of time for coupled kinetics. The comparison between the two chlorinated species shows the expected effect that the SiCl₂ desorption rate decreases more than the SiCl one during the laser pulse: while the SiCl desorption peak exhibits a large shoulder after the beginning of melting, the SiCl₂ desorption falls off rapidly. The SiCl shoulder is due to retrodiffused chlorine (from the bulk to the surface) during melting. SiCl₂ does not exhibit the shoulder because the Cl coverage is too low at that stage to yield a significant production of SiCl₂. We expect, therefore, that the saturation of the etch rate occurs more rapidly

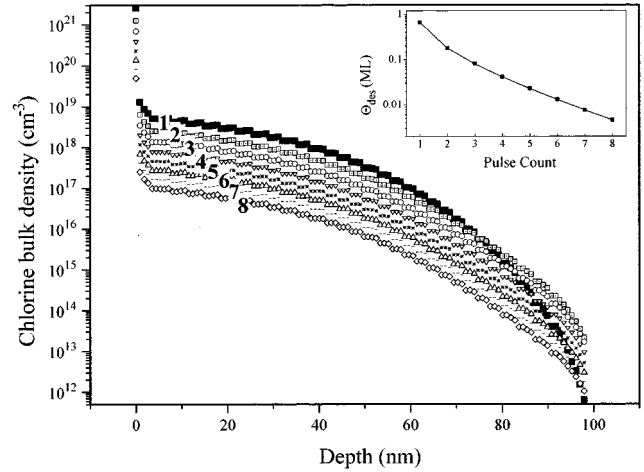


FIG. 10. Calculated chlorine depth profile after eight successive laser pulses. The initial coverage is 1 ML. There is no readsorption between laser pulses. The inset contains the total amount of desorbed Cl per pulse, Θ_{des} , vs pulse count. The parameters used in the calculation are those of Table I.

for a second-order desorption (for in the steady state of the liquid surface the desorption is nearly zero). This is confirmed in Fig. 8(b): the saturation of the etch rate as a function of laser fluence is achieved by including SiCl₂ second-order desorption. The results shown in Table I are in agreement with all available experimental data.

Separate kinetics. When “separate” kinetics are assumed, the results (Table II) are nearly identical with those of coupled kinetics (Table I) if we take the initial SiCl to SiCl₂ ratio to be $\eta = 3/7$. The etch rate dependence on laser fluence [Fig. 8(c)] is satisfactorily reproduced with this model.

Laser cleaning. In Fig. 10 we present the chlorine depth profile for a series of eight laser pulses. We set 1 ML before the first laser pulse. The final depth profile for one pulse becomes the initial profile for the next pulse. It can be observed that the shape of the chlorine depth profile becomes constant after about three pulses, the changes being small between pulses 1–3. After pulse 3, the profiles are simply translated on a log scale from pulse to pulse, showing that the desorption yield decreases like the logarithm of the laser count. This is shown in the inset of Fig. 10. The Cl content of the substrate decreases by a factor ≈ 1.6 at each pulse. It takes ≈ 5 laser pulses to decrease it by one order of magnitude.

TABLE II. Experimental and calculated results for the case of “separate” kinetics (see text, Sec. III C). Θ_{AES} and n_{SIMS} are the “surface Cl” and Cl concentrations in the eighth plane below the surface after the laser pulse, respectively. SiCl/SiCl₂ is the branching ratio between the desorption products. K_s is the segregation coefficient.

	E_1^l (eV)	E_2^l (eV)	E_2^s (eV)	Θ_{AES} (ML)	SiCl/SiCl ₂	Etch rate (Å/pulse) ^a	n_{SIMS} (10^{19} cm^{-3})	K_s
This work	1.9 ± 0.1^b	3.2 ± 0.1^c	3.7 ± 0.1	0.36	0.97	0.57	1.2	≤ 0.02
Experiment			3.61	0.37 ± 0.13	1.3 ± 0.3	0.56 ± 0.04	≤ 1.0	
			Ref. 8	Ref. 6	Ref. 6	Ref. 6	Ref. 6	

^aFor laser fluences above 500 mJ cm^{-2} .

^bAssuming a preexponential factor of 10^{14} s^{-1} .

^cAssuming a preexponential factor of $2 \times 10^3 \text{ cm}^2 \text{ s}^{-1}$.

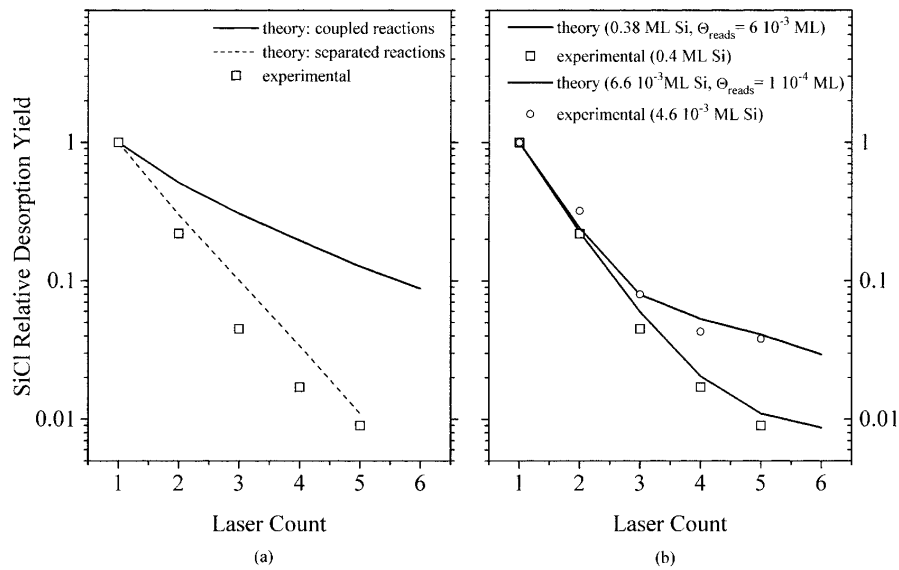


FIG. 11. (a) Experimental and calculated relative yield of SiCl desorption for a series of laser pulses at 600 mJ cm^{-2} . The surface is initially saturated with chlorine. Both coupled and separate kinetics are considered. The parameters used in the calculation are those of Tables I and II, respectively. (b) Experimental and calculated relative yield of SiCl desorption for a series of laser pulses at 600 mJ cm^{-2} . In the first set of experimental data, the surface is initially saturated with Cl, resulting in a Si desorption yield at the first pulse of 0.40 ML; a readsorption of 0.0060 ML of chlorine between the laser pulses is included in the calculation. In the second set of experimental data, the Si desorption yield at the first pulse is 4.6×10^{-3} ML; a readsorption of 0.0004 ML of chlorine between the laser pulses is included in the calculation. The parameters used in the calculation are those of Table I (coupled kinetics).

Multipulse experiments. Other experimental data can be considered to discriminate between coupled and separate kinetics: AES and TOF measurements of multipulse experiments. In these experiments, the initial coverage was varied, and consequently they should be more sensitive to the reaction order. The TOF results of Ref. 6 consist of a series of eight laser pulses following a single Cl_2 pulse which is provided by a molecular beam. As can be seen in Fig. 11(a), the coupled kinetics fail to reproduce the experimental results, whereas the separate kinetics succeed. It does because the nonlinearity in Cl coverage is more important in the separate kinetics than in the coupled kinetics. With coupled kinetics, first-order desorption dominates as soon as the Cl coverage and concentration decrease and the relative yield of SiCl desorption decreases more quickly with laser count in the calculation than experimentally. However, these results are not conclusive, because a constant Cl_2 pressure could not be avoided in the experiments in addition to the Cl_2 pulse. Taking into account the effect of the resulting weak readsorption between the laser pulses is sufficient to obtain a satisfactory agreement with experiment using the coupled kinetics [Fig. 11(b)].

In the AES experiments, the problem of readsorption is not encountered. The calculations with separate kinetics agree better with the experimental data than with coupled kinetics (Fig. 12).

V. DISCUSSION

Our model cannot go into the details of desorption. The available experimental data are not sufficient for this purpose. However, as it is, our model allows us to validate the conclusions drawn qualitatively in Ref. 6, and to quantify the processes of the segregation of Cl at the Si liquid-solid in-

terface, and of the desorption of silicon chlorides from liquid Si. The determination of the segregation coefficient, and of the activation energies of desorption, are highly constrained, and while a more refined model would provide different numbers, the order of magnitude of our results on segregation and desorption seem well established. The experimental data are not sufficient to discriminate between ‘‘coupled’’ or ‘‘separate’’ kinetics. However, both kinetics yield desorption energies of the same order of magnitude.

For the first-order kinetics, the desorption rate increases by a factor 60 at 2000 K upon melting. This change of the desorption rate is assigned in this paper to a change of the

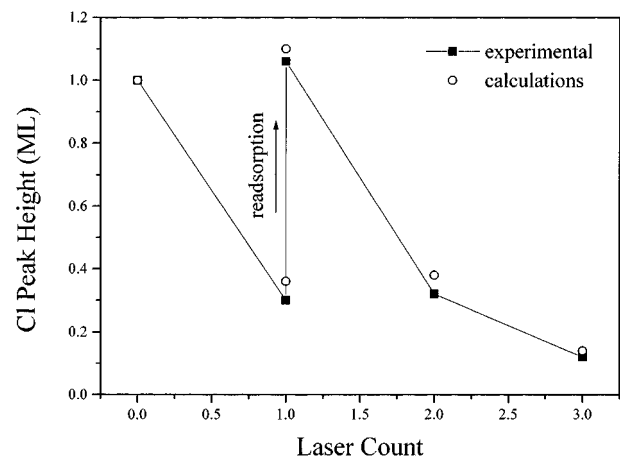
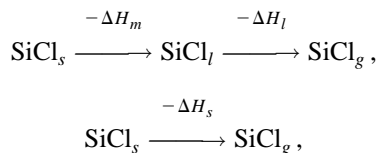


FIG. 12. Experimental and calculated AES Cl signal after (1) surface saturation by chlorine, (2) one single laser pulse, (3) resaturation of the surface by chlorine, (4) a second laser pulse, and (5) a third laser pulse. The parameters used in the calculation are those of Table II (separate kinetics).

desorption energy. The desorption energy should change, because on the liquid surface the local environment of Si atoms will adapt quickly as a molecule desorbs, so as to minimize the potential energy during desorption. This will not occur on the solid surface, where a reactive site is left behind by the desorbing molecule. However, a change of the pre-exponential factor with the state of the surface can also occur. It is usually believed (although not substantiated by experiments) that an increased mobility of the adsorbate reduces statistically the chances to desorb by a first-order kinetics and results in a *smaller* pre-exponential factor. It would have to be compensated for by an even larger decrease of the desorption energy. The respective role of the pre-exponential factor and the desorption energy could only be unraveled by a measurement of the desorption rate with the surface temperature, which seems very difficult to do because the peak temperature is only calculated, and because it varies little with the laser fluence. Because of these difficulties, we discuss the meaning of the change of the desorption energies with the assumption that the pre-exponential factors do not change.

The activation energies for desorption that we obtain for the *solid* surface can be compared directly with the literature on thermal desorption, and the agreement is quite satisfactory. There are no such data to compare with for *liquid* Si, and it is an important result of the present work to provide desorption energies for liquid Si, we believe for the first time. The difference between the energies for the solid and liquid is found to be 0.7 ± 0.2 eV for first-order desorption, and 0.4 ± 0.2 or 0.5 ± 0.2 (depending on the kinetics, coupled or separate) for second-order desorption. It is worth noting that the experimental value of the heat of melting of silicon [0.52 eV (Ref. 22)] is within the uncertainty limits. Let us consider the following reaction scheme:



where ΔH_m is the latent heat of melting of the SiCl overlayer, while ΔH_s and ΔH_l are the heats of desorption from the solid and liquid surfaces, respectively. Assuming that ΔH_m can be approximated by the latent heat of solid Si, we obtain the result that $\Delta H_s = \Delta H_m + \Delta H_l$, which seems to be verified experimentally. Alternatively, a more accurate determination of ΔH_m would allow to measure small effects that change ΔH_m , like the strain of the solid surface.²³

Because desorption on the solid surface occurs through the diffusion-limited formation of SiCl₂, it could be assumed that it is the strongly increased diffusion on the liquid surface that results in the observed large etch rate above the melting threshold. In fact, SiCl desorbs as efficiently as SiCl₂, the desorption of both products being easier on the liquid surface. The increased diffusion does not facilitate the production of SiCl₂ because it also has the effect of scattering Cl in the whole melted layer.

Our program allows us to calculate features that were not, or that cannot be measured experimentally, like the Cl coverage at the surface and the Cl depth profile (Fig. 13) as a function of time, or the kinetics of cleaning as a function of

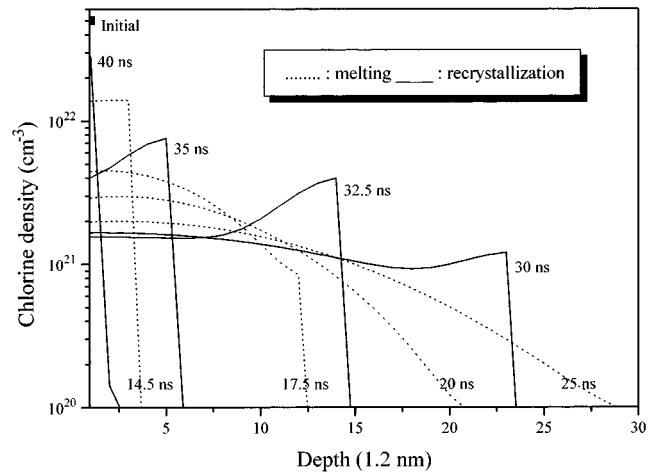


FIG. 13. Calculated chlorine depth profile at different times of melting for a laser fluence of 600 mJ cm^{-2} and for the coupled kinetics (Table I).

laser count. The former shows that desorption and etching occur in a fraction of a nanosecond at the beginning of melting. It follows that the excess energy is not used at all for etching. This explains why the etch rate dependence on laser fluence so quickly reaches a saturation after the sharp increase above the melting threshold. The latter is illustrated in Fig. 10, and it shows an important feature of laser cleaning: while the branching ratio favors desorption in the case of 1 ML of Cl on a clean Si substrate (about two-thirds of Cl atoms are desorbed⁶), it is less favorable from the point of view of cleaning when the atoms are initially distributed in the volume. The desorbed fraction of Cl per laser pulse stabilizes to $\approx \frac{1}{3}$ after three laser pulses. As is shown in Figs. 4 and 5, the desorption occurs at the very beginning of melting, and only molecules at, or close to, the surface, can desorb: the mechanism of laser cleaning is the desorption of surface species, followed by the redistribution of the remaining impurities. At this stage (which prepares the desorption at the next pulse), segregation plays a key role. We have observed this for O and C on Si. It takes a few thousand pulses to decrease the coverage of the former below the sensitivity level of AES, while it takes less than ten pulses to obtain the same result for the latter.⁶ O does not segregate at all on Si, while C does. The level of Cl contamination indicated in this paper and in Ref. 6 is only an upper limit. Quite possibly, the Cl concentration after etching is lower than 10^{19} cm^{-3} , and the segregation coefficient would then be even smaller than 0.02.

The Cl segregation is very strong even at a speed of recrystallization of ≈ 6 ms. As a consequence, the Cl depth profile is very sharp (Fig. 13). This is unusual. Si dopants which have a small segregation coefficient at equilibrium exhibit a weak segregation (Sb), if any at all (As), at such a speed of recrystallization. This is why laser annealing is an interesting tool to obtain concentrations of dopants larger than solubilities in substitutional sites.⁵ Most probably, the strong segregation of Cl is due to the fact that Cl cannot be substituted to Si atoms, because of its electronic structure (it belongs to group VII), and it cannot either be placed in interstitial sites (unlike F) because it is too large.

VI. CONCLUSIONS

The pulsed-laser etching of silicon by chlorine is described quantitatively. Calculations include desorption in addition to heat and mass transport. The results allow us to simulate successfully a large set of available experimental data (AES, TOF, and SIMS) that put rather large constraints on the fitted parameters. The segregation coefficient of Cl at the Si liquid-solid interface, and the activation energies for desorption from the liquid, are obtained. The difference of the activation energies on the liquid and solid is within experimental uncertainty equal to the latent heat of melting of Si. The diffusion of the initially adsorbed chlorine below the surface is confirmed to be a limiting factor of the etching. The experimentally observed saturation of laser etching is also influenced by the SiCl/SiCl₂ branching ratio and by kinetic details of desorption (i.e., the reaction order). The time scale of desorption is a fraction of a nanosecond. The laser cleaning efficiency is shown to depend critically on the seg-

regation coefficient; in the case of Cl on Si, the desorbed fraction decreases from $\approx \frac{2}{3}$ to $\approx \frac{1}{3}$ per laser pulse in the three first pulses, and then it is stable. Our treatment of desorption can be used for a variety of other adsorbate-substrate systems. For example, it is known that dopants like Sb can desorb rather efficiently during Si etching.⁵ The prediction of the number of laser pulses necessary for the cleaning of C and O impurities at levels beyond the sensitivity of AES can also be done. However, a more basic development of this work is to couple the heat and mass flow calculations in order to understand the role of impurities on the dynamics of surface melting. Significantly improved data on the thermal and optical properties of silicon would be gained. The experimental task is to measure more accurately, and on a better controlled substrate, the melting dynamics in a single laser pulse. Possibly, the determination of a quantity like ΔH_m , that involves the change of the latent heat by strain or other adsorbate-induced effects, could be obtained.

*Corresponding author. Electronic address:

Bernard.Bourguignon@ppm.u-psud.fr

¹R. F. Wood and G. E. Giles, Phys. Rev. B **23**, 2923 (1981).

²J. R. Wood, J. R. Kirkpatrick, and G. E. Giles, Phys. Rev. B **23**, 5555 (1981).

³S. U. Campisano, Appl. Phys. A **30**, 195 (1983).

⁴J. Boulmer, J.-P. Budin, B. Bourguignon, D. Débarre, and A. Desmur, in *Laser Ablation of Electronic Materials*, edited by E. Fogarassy and S. Lazare (Elsevier, Amsterdam, 1992), p. 239.

⁵A. Desmur, B. Bourguignon, J. Boulmer, J.-B. Ozenne, J.-P. Budin, D. Débarre, and A. Aliouchouche, J. Appl. Phys. **76**, 3081 (1994).

⁶B. Bourguignon, M. Stoica, B. Dragnea, S. Carrez, J. Boulmer, J.-P. Budin, D. Débarre, and A. Aliouchouche, Surf. Sci. **338**, 94 (1995).

⁷R. F. Wood, Phys. Rev. B **25**, 2786 (1982).

⁸A. Szabo, P. D. Farrall, and T. Engel, Surf. Sci. **312**, 284 (1994).

⁹R. B. Jackman, H. Ebert, and J. S. Foord, Surf. Sci. **176**, 183 (1986).

¹⁰M. Seel and P. S. Bagus, Phys. Rev. B **28**, 2023 (1983).

¹¹T. D. Durbin, W. C. Simpson, V. Chakarian, D. K. Shuh, P. R. Varekamp, C. W. Lo, and J. A. Yarmoff, Surf. Sci. **306**, 257 (1994).

¹²L. S. Johansson, R. I. G. Uhrberg, R. Lindsay, P. L. Wincott, and G. Thornton, Phys. Rev. B **42**, 9534 (1990).

¹³D. Sterratt, C. L. Greenwood, E. M. Williams, C. A. Huryn, P. L. Wincott, G. Thornton, and E. Roman, Surf. Sci. **307–309**, 269 (1994).

¹⁴Q. Gao, C. C. Cheng, P. J. Chen, W. J. Choyke, and J. T. Yates, Jr., J. Chem. Phys. **98**, 8308 (1993).

¹⁵J. Matsuo, F. Yannick, and K. Karahashi, Surf. Sci. **283**, 52 (1993).

¹⁶P. Gupta, P. A. Coon, B. G. Koehler, and S. M. George, Surf. Sci. **249**, 92 (1991).

¹⁷S. De Unamuno and E. Fogarassy, Appl. Surf. Sci. **36**, 1 (1989).

¹⁸J. J. Bruines, Ph.D. thesis, Technical University of Eindhoven, 1988.

¹⁹G. E. Jellison, Jr., A. Modine, Phys. Rev. B **27**, 7466 (1983).

²⁰J. Boulmer, B. Bourguignon, J.-P. Budin, D. Débarre, and A. Desmur, J. Vac. Sci. Technol. A **9**, 2923 (1991).

²¹D. P. Brunco, M. O. Thompson, D. F. Hoglund, M. J. Aziz, and H.-J. Gossmann, J. Appl. Phys. **78**, 1575 (1995).

²²F. F. Abraham and J. Q. Broughton, Phys. Rev. Lett. **56**, 734 (1986).

²³J. Tersoff, Phys. Rev. Lett. **74**, 5080 (1995).